Optics Letters

Anharmonic propagation of two-dimensional beams carrying orbital angular momentum in a harmonic potential

Yiqi Zhang,[1,4] Xing Liu,[1] Milivoj R. Belić,[2,5] Weiping Zhong,[3] Feng Wen,[1] and Yanpeng Zhang[1,6]

[1]Key Laboratory for Physical Electronics and Devices of the Ministry of Education & Shaanxi Key Lab of Information Photonic Technique, Xi'an Jiaotong University, Xi'an 710049, China
[2]Science Program, Texas A&M University at Qatar, P.O. Box 23874 Doha, Qatar
[3]Department of Electronic and Information Engineering, Shunde Polytechnic, Shunde 528300, China
[4]e-mail: zhangyiqi@mail.xjtu.edu.cn
[5]e-mail: milivoj.belic@qatar.tamu.edu
[6]e-mail: ypzhang@mail.xjtu.edu.cn

Received 23 June 2015; accepted 17 July 2015; posted 21 July 2015 (Doc. ID 242661); published 7 August 2015

We analytically and numerically investigate an anharmonic propagation of two-dimensional beams in a harmonic potential. We pick noncentrosymmetric beams of common interest that carry orbital angular momentum. The examples studied include superposed Bessel–Gauss (BG), Laguerre–Gauss (LG), and circular Airy (CA) beams. For the BG beams, periodic inversion, phase transition, and rotation with periodic angular velocity are demonstrated during propagation. For the LG and CA beams, periodic inversion and variable rotation are still there but not the phase transition. On the whole, the "center of mass" and the orbital angular momentum of a beam exhibit harmonic motion, but the motion of the beam intensity distribution in detail is subject to external and internal torques and forces, causing it to be anharmonic. Our results are applicable to other superpositions of finite circularly asymmetric beams.

OCIS codes: (070.3185) Invariant optical fields; (070.0070) Fourier optics and signal processing; (350.5500) Propagation.

http://dx.doi.org/10.1364/OL.40.003786

In the last decade, accelerating beams, such as Airy and related beams, have attracted much attention and were intensively investigated. Dynamics of Airy beams were considered in free space [1,2], bulk nonlinear media [3–7], fibers [8–12], media with external potentials [13–18], and so on. In an external potential, naturally, the spatial properties of Airy beams will be modulated during propagation. In a recent article, we showed that a one-dimensional (1D) finite-energy Airy beam will, quite surprisingly, perform periodic inversion, phase transition, and anharmonic oscillation during propagation in a harmonic potential [18]. Under phase transition, we mean the transition of the optical mode from one form to another during propagation. A natural question is, will this behavior carry over to two dimensions?

In the paper mentioned [18], toward the end, we proved that the 2D case of an Airy beam can be reduced to the product of two 1D cases, on the account of the linearity of the problem. Thus, a product of two finite-energy Airy beams—one along x and the other along y direction—will in a two-dimensional parabolic potential exhibit all the properties of 1D Airy beams: periodic inversion, phase transition, and anharmonic oscillation. However, the interest in 2D goes beyond the products of 1D beams—to the genuine 2D beams that can be radially symmetric or asymmetric and importantly, can carry orbital angular momentum.

On the other hand, recently radially self-accelerating [19] and angularly accelerating [20] beams have been introduced. In these papers, beams that carry angular momentum, related to Bessel waves—which are also nondiffracting [21–23]—have been propagated in free space. In a similar vein, we want to know what happens to an asymmetric diffractionless beam, which carries orbital angular momentum, when launched into a harmonic potential. The beam will also radially and angularly accelerate, but what modulation will it receive and how will it behave in such a common potential? Do phase transition and periodic inversion carry over from one dimension, and how are they affected by the rotation imposed on the beam? For the difference, instead of considering exotic beams such as helicons [19] or superpositions of vortices with opposite helicities [20], we focus on familiar beams such as Bessel–Gauss (BG), Laguerre–Gauss (LG), and circular Airy (CA) beams.

Hence, in this Letter, we construct two-dimensional beams by superposing several BG and LG beams of different order, and investigate their dynamics as they propagate in a harmonic potential. In addition, we also discuss the propagation of a superposition of rotating CA beams with different topological charges. To consider more interesting cases of rotating asymmetric intensity distributions, we chose the BG, LG, and CA beams in the form of noncentrosymmetric superpositions.

Such superpositions more readily expose the effects we are after, which also depend on the internal structure of beams. Thus, we suppose that the evolution of a 2D beam can be understood as a variable rotation of its intensity distribution, which can be described in terms of beam's moment of inertia and its angular velocity [21]. In an external potential, there appear external torques and forces acting on the beam, and the orbital angular momentum is not conserved. In addition, there exist internal forces and torques that change the intensity distribution internally, whose evolution then appears anharmonic.

In the paraxial approximation and in the harmonic potential, the beam in propagation obeys the dimensionless linear (2 + 1)D Schrödinger equation

$$i\frac{\partial\psi}{\partial z}+\frac{1}{2}\nabla^2\psi-\frac{1}{2}\alpha^2(x^2+y^2)\psi=0, \tag{1}$$

where ψ is the beam envelope and α a parameter controlling the width of the potential. The variables x, y, and z are the normalized transverse coordinates and the propagation distance, scaled by some characteristic transverse width $x_0=y_0$ and the corresponding Rayleigh range kx_0^2. Here, $k=2\pi n/\lambda_0$ is the wavenumber, n the ambient index of refraction, and λ_0 the wavelength in free space. Typically, the external harmonic potential comes from the modulation of the index of refraction, easily achieved, for example, in gradient-index (GRIN) media.

With this choice of the potential, Eq. (1) describes the linear 2D harmonic oscillator and possesses many well-known solutions. In Fourier optics, one is interested in the solutions that can be written as [18]

$$\psi(x,y,z)=-\frac{i}{2\pi}f(x,y,z)\iint_{-\infty}^{+\infty}\mathrm{d}\xi\mathrm{d}\eta\psi(\xi,\eta)$$
$$\times\exp[ib(\xi^2+\eta^2)]\exp[-iK(x\xi+y\eta)], \tag{2}$$

where $f(x,y,z)=K\exp[ib(x^2+y^2)]$, $b=\alpha\cot(\alpha z)/2$, and $K=\alpha/\sin(\alpha z)$. It is clear that the integral in Eq. (2) is the 2D Fourier transform of $\psi(\xi,\eta)\exp[ib(\xi^2+\eta^2)]$, with Kx and Ky being the spatial frequencies.

As an example, we consider an input in the form of a superposition of BG beams:

$$\psi(r,\theta)=\sum_{n=1}^{4}J_n(ar)\exp(in\theta)\exp\left(-\frac{r^2}{\sigma^2}\right), \tag{3}$$

in which σ is the decay factor, $J_n(\bullet)$ represents the Bessel function of the first kind of order n, and a is an arbitrary stretching coefficient. The intensity following from Eq. (3) is noncentrosymmetric. The oscillating period is $\mathcal{D}=2\pi/\alpha$ [18].

Plugging the input given by Eq. (3) into Eq. (2), one obtains

$$\psi(r,\theta,z)=-\frac{i}{2\pi}f(r,\theta,z)\int_0^{+\infty}\int_0^{2\pi}\rho\mathrm{d}\rho\mathrm{d}\phi$$
$$\times\sum_{m=-\infty}^{+\infty}i^{-m}J_m(\rho r)\exp(-im\phi)\exp(im\theta)$$
$$\times\sum_{n=1}^{4}g_n(\rho)\exp(in\phi), \tag{4}$$

where

$$g_n(\rho)=J_n(a\rho)\exp(ib\rho^2)\exp\left(-\frac{\rho^2}{\sigma^2}\right).$$

Here, $\rho^2=\xi^2+\eta^2$ and $\phi=\arctan(\eta/\xi)$ represent the spatial polar coordinates, and $r^2=K^2(x^2+y^2)$ and $\theta=\arctan(y/x)$ represent the spatial frequency in polar coordinates. In Eq. (4), we utilize the relation [24]

$$\exp[-iK(x\xi+y\eta)]=\sum_{m=-\infty}^{+\infty}i^{-m}J_m(\rho r)\exp(-im\phi)\exp(im\theta).$$

By introducing the Kronecker delta,

$$\int_0^{2\pi}\exp[i(n-m)\phi]\mathrm{d}\phi=2\pi\delta_{nm}=\begin{cases}0 & \text{if } n\neq m\\ 2\pi & \text{if } n=m,\end{cases}$$

Eq. (4) can be rewritten as

$$\psi(r,\theta,z)=-f(r,\theta,z)\sum_{n=1}^{4}i^{1-n}\exp(in\theta)\int_0^{+\infty}g_n(\rho)J_n(\rho r)\rho\mathrm{d}\rho. \tag{5}$$

As a result, the final solution can be written as [25]

$$\psi(r,\theta,z)=-\frac{1}{2w}f(r,\theta,z)$$
$$\times\sum_{n=1}^{4}i^{1-n}\exp(in\theta)\exp\left(-\frac{r^2+a^2}{4w}\right)I_n\left(\frac{ar}{2w}\right), \tag{6}$$

where $w=1/\sigma^2-ib$ and $I_n(\bullet)$ is the modified Bessel function of the first kind of order n.

Figure 1 depicts the propagation of the finite energy BG beam with $a=4$ and $\sigma=10$ in a harmonic potential. From the panels, one can clearly see the periodic inversion of the beam during propagation. In the 3D plot below panels, one can discern two separate phases in the evolution of the beam. Specifically, the panel in Fig. 1(c)—the second phase of the

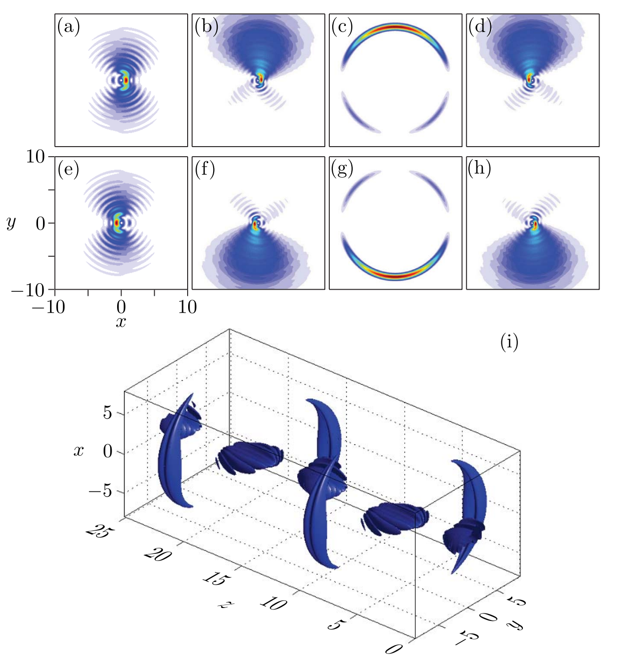

Fig. 1. Intensity of the Bessel–Gauss beam during propagation in a harmonic potential with $\alpha=0.5$ at $z=0$ (a), $\mathcal{D}/8$ (b), $\mathcal{D}/4$ (c), $3\mathcal{D}/8$ (d), $\mathcal{D}/2$ (e), $5\mathcal{D}/8$ (f), $3\mathcal{D}/4$ (g), and $7\mathcal{D}/8$ (h), respectively. (i) Iso-surface plot (Visualization 1) of the propagation.

beam—is the Fourier transform of the initial beam from Fig. 1(a). It is equivalent to a superposition of perfect vortex beams of different order [26]. Based on Eq. (5), the analytical intensity distribution can be obtained (not shown), which is in complete accordance with the numerical simulation. In Fig. 1(i) we display the iso-surface plot of the beam during propagation. One can note that the beam undergoes periodic inversion and two-phase oscillation. We would like to point that, similar to the finite-energy Airy beams [18], the oscillation of the maximum intensity is anharmonic. Visualization 1 provides a clear animated version of this propagation. Thus, the periodic inversion and the two-phase oscillation of an asymmetric BG beam are clearly seen during propagation.

Equation (5) is an analytical solution, with $\psi(r,\theta)$ being the input. An analogous procedure is feasible for other kinds of inputs, e.g., a superposition of finite LG beams of different order [27]:

$$\psi(r,\theta) = \sum_{n=1}^{4} A r^n L_n^n(ar^2)\exp(in\theta)\exp\left(-\frac{r^2}{\sigma^2}\right), \tag{7}$$

where the generalized Laguerre polynomial is $L_n^t(x) = x^{-t}e^x/n!d^n(e^{-x}x^{n+t})/dx^n$, and A is the amplitude. Plugging Eq. (7) into Eq. (2), and following the same procedure as for the BG beams, one obtains the corresponding solution, which can be written as [25]

$$\psi(r,\theta,z) = -\frac{A}{2w} f(r,\theta,z)\exp\left(-\frac{r^2}{4w}\right) \times \sum_{n=1}^{4} i^{1-n}\exp(in\theta)\left(\frac{w-a}{2w^2}r\right)^n L_n^n\left[\frac{ar^2}{4w(a-w)}\right]. \tag{8}$$

For convenience, we assume $a=1$, $\sigma=\sqrt{2}$, and $A=0.1$ (in a linear system, the value of A is arbitrary). In Figs. 2(a)–2(h), we display the intensity distributions of the beam at certain distances, while in Fig. 2(i) and Visualization 2, we show the propagating dynamics of the whole beam. From Fig. 2 and Visualization 2, one can see that the LG beam rotates anticlockwise during propagation, without changing basically its profile. The reason is clear: from Eq. (8), one sees that the propagating beam is again a superposition of LG beams but with different parameters. As a result, the two-phase oscillation disappears in Fig. 2.

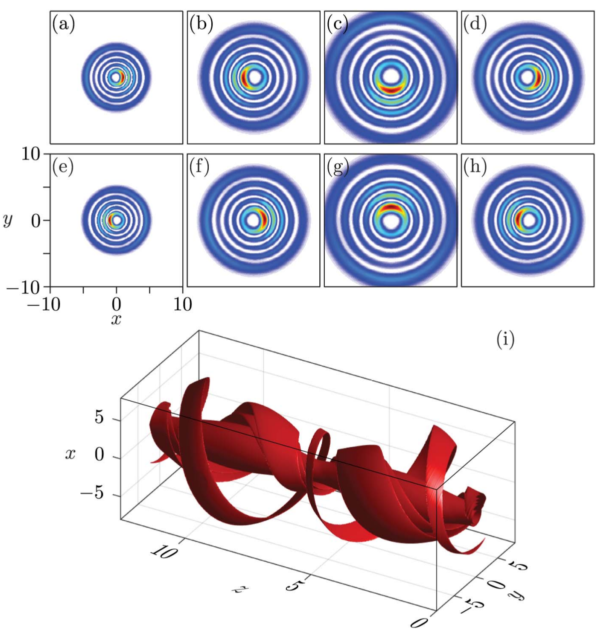

Fig. 2. Laguerre–Gauss beam in propagation. Figure setup is as in Fig. 1.

As mentioned before, a 2D Airy beam can be considered as a product of two 1D Airy beams. Thus, it displays inversion and phase transition during propagation [18]. We want to check the behavior of a 2D Airy beam when it rotates. To this end, we turn to the propagation of superposed CA beams [28–32]:

$$\psi(r,\theta) = Ai[\pm(r-r_0)]\exp[\pm a(r-r_0)]\sum_{n=1}^{4}\exp(in\theta), \tag{9}$$

where a is the decay factor, r_0 determines the center of the main ring, and $\pm$ corresponds to the inward and outward CA beams, respectively. Unfortunately, an analytical solution corresponding to the propagating input beam from Eq. (9) is hard to obtain. To handle such a difficult problem, a fairly accurate approximation was developed in [29]. The result is that the CA beam during propagation can be approximated by

$$\psi(r,\theta,z) \approx -A_0 f(r,\theta,z)\exp(ibr_0^2)\sum_{n=1}^{4} i^{1-n}\exp(in\theta)J_n(r_0 r), \tag{10}$$

where $A_0 \approx (1-a^2/r_0)\exp(a^3/3)$. Clearly, Eq. (10) is a superposition of Bessel beams of the first kind, and the propagation of such a beam should be similar to Fig. 1. The result is depicted in Fig. 3.

In the figure, we display the intensity distributions of outward CA beams [Figs. 3(a)–3(d)] and inward CA beams [Figs. 3(e)–3(h)] at certain distances. In Figs. 3(b) and 3(d) for outward, and Figs. 3(f) and 3(h) for inward CA beams, the intensity recorded at $z = \mathcal{D}/4$ indeed is similar to that shown in Fig. 1(a). This holds for both inward and outward CA beams, because Eq. (10) is not limited to only one kind of CA beams. However, the two-phase transition seems to be absent. Therefore, analytical results agree with numerical simulations quite well. In Fig. 3(i) (and Visualization 4), we display the isosurface plot of the propagation, which corresponds to the inward CA beams. For CA beams, the oscillation is more continuous, similar to LG beams.

In the end, it is instructive to look at the dynamics of the "center of mass" [18,21], coming from the intensity distribution

$$\bar{x} = \frac{\iint_{-\infty}^{+\infty} x|\psi|^2 \mathrm{d}x\mathrm{d}y}{\iint_{-\infty}^{+\infty} |\psi|^2 \mathrm{d}x\mathrm{d}y}, \qquad \bar{y} = \frac{\iint_{-\infty}^{+\infty} y|\psi|^2 \mathrm{d}x\mathrm{d}y}{\iint_{-\infty}^{+\infty} |\psi|^2 \mathrm{d}x\mathrm{d}y},$$

and the dynamics of the orbital angular momentum [33,34]

$$L_z = -\frac{i}{2}\iint_{-\infty}^{+\infty}\psi^*\left(x\frac{d\psi}{dy} - y\frac{d\psi}{dx}\right)\mathrm{d}x\mathrm{d}y + \mathrm{c.c.}$$

of noncentrosymmetric beams. These beams carry orbital angular momentum and rotate during propagation. This momentum is proportional to the product of the moment of inertia of the beam and its angular velocity that in turn may both depend on the propagation distance. Such a dependence produces a

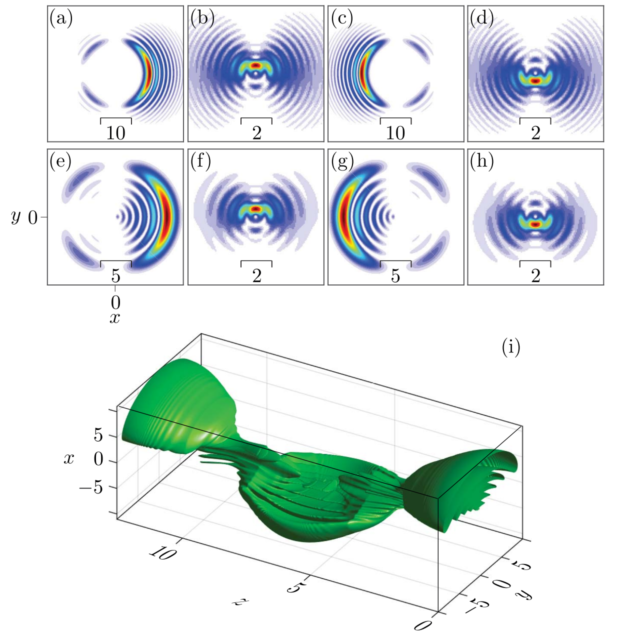

Fig. 3. Propagation of circular Airy beams. From left to right: intensity distributions at $z = 0$, $z = \mathcal{D}/4$, $z = \mathcal{D}/2$, and $z = 3\mathcal{D}/4$. Intervals inside give the relative measure of the beam size. (a)–(d) Outward CA beam (Visualization 3). (e)–(h) Inward CA beam (Visualization 4). (i) Iso-surface plot of the propagation of the inward CA beam. Parameters: $\alpha = 0.5$, $a = 0.1$ and $r_0 = 10$.

torque on the beam that exhibits components along both the angular velocity and the angular acceleration. The force acting on the beam in such a rotation is not uniform along the propagation coordinate and imparts radial and angular acceleration to the beam, resulting in a nonuniform periodic behavior (results not shown). Hence, the beam cannot be classified as a purely angularly or purely radially accelerating beam, because these kinds of beams require certain conditions [19].

In summary, we have investigated the dynamics of superposed two-dimensional BG, LG, and CA beams in a medium with an external harmonic potential. Due to orbital angular momentum, beams rotate during propagation, with the intensity and the angular velocity changing periodically. The BG beams exhibit phase transition at an odd-integer multiple of quarters of the oscillation period, and undergo spatial inversion at an odd-integer multiple of halves of the period. For the LG beams, the two-phase oscillation disappears, and the beam profile does not change significantly, because it is always described by a superposition of LG beams of the same order but different parameters. Concerning CA beams, the propagation looks similar to that of LG beams, but is approximately described by the superposition of Bessel beams.

In general, the analytical solution described in this Letter is applicable to other noncentrosymmetric initial beams composed of finite circularly symmetric components. Periodic inversion and anharmonic oscillation appear to be universal features of propagation in the harmonic potential, but the appearance of two-phase oscillation depends on the actual beam distribution. Our investigation may lead to potential applications in particle manipulation, signal processing, propagation in GRIN media, and other fields.

Funding. Key Scientific and Technological Innovation Team of Shaanxi Province (2014KCT-10); National Basic Research Program of China (2012CB921804); National Natural Science Foundation of China (NSFC) (11474228, 61308015); Natural Science Foundation of Shaanxi Province (2014JQ8341); Qatar National Research Fund (NPRP 6-021-1-005).

Acknowledgment. Yiqi Zhang appreciates the anonymous referees for their constructive comments to improve the Letter.

REFERENCES

1. G. A. Siviloglou and D. N. Christodoulides, Opt. Lett. **32**, 979 (2007).
2. G. Siviloglou, J. Broky, A. Dogariu, and D. Christodoulides, Phys. Rev. Lett. **99**, 213901 (2007).
3. Y. Q. Zhang, M. Belić, Z. K. Wu, H. B. Zheng, K. Q. Lu, Y. Y. Li, and Y. P. Zhang, Opt. Lett. **38**, 4585 (2013).
4. Y. Q. Zhang, M. R. Belić, H. B. Zheng, H. X. Chen, C. B. Li, Y. Y. Li, and Y. P. Zhang, Opt. Express **22**, 7160 (2014).
5. G. Zhou, R. Chen, and G. Ru, Laser Phys. Lett. **11**, 105001 (2014).
6. R. Driben, V. V. Konotop, and T. Meier, Opt. Lett. **39**, 5523 (2014).
7. M. Shen, J. Gao, and L. Ge, Sci. Rep. **5**, 9814 (2015).
8. I. Besieris and A. Shaarawi, Phys. Rev. E **78**, 046605 (2008).
9. R. Driben, Y. Hu, Z. Chen, B. A. Malomed, and R. Morandotti, Opt. Lett. **38**, 2499 (2013).
10. R. Driben and T. Meier, Phys. Rev. A **89**, 043817 (2014).
11. S. Wang, D. Fan, X. Bai, and X. Zeng, Phys. Rev. A **89**, 023802 (2014).
12. L. Zhang, K. Liu, H. Zhong, J. Zhang, Y. Li, and D. Fan, Opt. Express **23**, 2566 (2015).
13. M. A. Bandres and J. C. Gutiérrez-Vega, Opt. Express **15**, 16719 (2007).
14. N. K. Efremidis, Opt. Lett. **36**, 3006 (2011).
15. W. Liu, D. N. Neshev, I. V. Shadrivov, A. E. Miroshnichenko, and Y. S. Kivshar, Opt. Lett. **36**, 1164 (2011).
16. Z. Ye, S. Liu, C. Lou, P. Zhang, Y. Hu, D. Song, J. Zhao, and Z. Chen, Opt. Lett. **36**, 3230 (2011).
17. N. K. Efremidis, Phys. Rev. A **89**, 023841 (2014).
18. Y. Q. Zhang, M. R. Belić, L. Zhang, W. P. Zhong, D. Y. Zhu, R. M. Wang, and Y. P. Zhang, Opt. Express **23**, 10467 (2015).
19. C. Vetter, T. Eichelkraut, M. Ornigotti, and A. Szameit, Phys. Rev. Lett. **113**, 183901 (2014).
20. C. Schulze, F. S. Roux, A. Dudley, R. Rop, M. Duparré, and A. Forbes, Phys. Rev. A **91**, 043821 (2015).
21. A. Bekshaev, M. S. Soskin, and M. Vasnetsov, *Paraxial Light Beams with Angular Momentum* (Nova Science, 2008).
22. J. Durnin, J. Opt. Soc. Am. A **4**, 651 (1987).
23. J. Durnin, J. J. Miceli, and J. H. Eberly, Phys. Rev. Lett. **58**, 1499 (1987).
24. N. Baddour, Adv. Imaging Electron Phys. **165**, 1 (2011).
25. I. Gradshteyn and I. Ryzhik, *Table of Integrals, Series, and Products*, 7th ed. (Academic, 2007).
26. P. Vaity and L. Rusch, Opt. Lett. **40**, 597 (2015).
27. D. Buccoliero, A. S. Desyatnikov, W. Krolikowski, and Y. S. Kivshar, Phys. Rev. Lett. **98**, 053901 (2007).
28. C.-Y. Hwang, K.-Y. Kim, and B. Lee, Opt. Express **19**, 7356 (2011).
29. P. Zhang, J. Prakash, Z. Zhang, M. S. Mills, N. K. Efremidis, D. N. Christodoulides, and Z. Chen, Opt. Lett. **36**, 2883 (2011).
30. I. Chremmos, P. Zhang, J. Prakash, N. K. Efremidis, D. N. Christodoulides, and Z. Chen, Opt. Lett. **36**, 3675 (2011).
31. C. Y. Hwang, K. Y. Kim, and B. Lee, IEEE Photon. J. **4**, 174 (2012).
32. P. Panagiotopoulos, D. G. Papazoglou, A. Couairon, and S. Tzortzakis, Nat. Commun. **4**, 2622 (2013).
33. Y. Q. Zhang, S. Skupin, F. Maucher, A. G. Pour, K. Q. Lu, and W. Królikowski, Opt. Express **18**, 27846 (2010).
34. M. S. Petrović, D. M. Jović, M. R. Belić, and S. Prvanović, Phys. Rev. A **76**, 023820 (2007).